Biophysical *Journal*
Article

Biophysical Society

The structural basis of Akt PH domain interaction with calmodulin

Jackson Weako,[1] Hyunbum Jang,[2] Ozlem Keskin,[3] Ruth Nussinov,[2,4,*] and Attila Gursoy[5,*]
[1]Computational Science and Engineering Program, Koç University, Istanbul, Turkey; [2]Computational Structural Biology Section, Frederick National Laboratory for Cancer Research in the Laboratory of Cancer Immunometabolism, National Cancer Institute, Frederick, Maryland; [3]Department of Chemical and Biological Engineering, Koç University, Istanbul, Turkey; [4]Department of Human Molecular Genetics and Biochemistry, Sackler School of Medicine, Tel Aviv University, Tel Aviv, Israel; and [5]Department of Computer Engineering, Koç University, Istanbul, Turkey

ABSTRACT Akt plays a key role in the Ras/PI3K/Akt/mTOR signaling pathway. In breast cancer, Akt translocation to the plasma membrane is enabled by the interaction of its pleckstrin homology domain (PHD) with calmodulin (CaM). At the membrane, the conformational change promoted by PIP_3 releases CaM and facilitates Thr308 and Ser473 phosphorylation and activation. Here, using modeling and molecular dynamics simulations, we aim to figure out how CaM interacts with Akt's PHD at the atomic level. Our simulations show that CaM-PHD interaction is thermodynamically stable and involves a β-strand rather than an α-helix, in agreement with NMR data, and that electrostatic and hydrophobic interactions are critical. The PHD interacts with CaM lobes; however, multiple modes are possible. IP_4, the polar head of PIP_3, weakens the CaM-PHD interaction, implicating the release mechanism at the plasma membrane. Recently, we unraveled the mechanism of PI3Kα activation at the atomistic level and the structural basis for Ras role in the activation. Here, our atomistic structural data clarify the mechanism of how CaM interacts, delivers, and releases Akt—the next node in the Ras/PI3K pathway—at the plasma membrane.

SIGNIFICANCE Akt is a principal component in the Ras/PI3K/Akt/mTOR pathway, translocating to the plasma membrane by calmodulin that releases autoinhibition. At the membrane, PIP_3 binding releases calmodulin, facilitating phosphorylation of Thr308 at the activation loop by PDK1 and Ser473 in the C-terminal tail by mTORC2, fully activating Akt. Inspired by the recent observation that calmodulin activates Akt in breast cancer, we performed MD simulations of multiple docking models, demonstrating that multiple modes of the calmodulin interactions with Akt-PHD are possible. Although the CaM-PHD association is thermodynamically favorable, IP_4 attenuates the interaction, clarifying the release mechanism at the plasma membrane. The details of the CaM-PHD release mechanism obtained uncover a potentially promising therapeutic strategy for breast and other related cancer types.

INTRODUCTION

The Akt protein (protein kinase B), a serine/threonine kinase, belongs to the AGC family (PKA, PKC, and PKG) of protein kinases. The family consists of over 60 evolutionarily related Ser/Thr protein kinases, most of which are modulated by phosphorylation of the C-terminal and the activation loop (1,2). Among the diverse signaling proteins, Akt has drawn vast attention. Through its numerous cellular substrates, Akt regulates cell survival, suppressing apoptosis and glucose metabolism. Its activation is associated with growth and survival signals, which physiologically are initiated at the cell surface by receptor-ligand interactions (3–5). The Akt1, Akt2, and Akt3 isoforms are products of different genes. They are very closely related and conserved. However, they exhibit function-specific differences in cell proliferation, apoptosis, and migration in human cancers (6–9). Hyperactivation of Akt1 promotes cancer and tissue overgrowth disorders (10,11). By contrast, inactivation of Akt2 is associated with insulin resistance in model organisms (12) and inherited diabetes in humans due to mutations (13), whereas Akt3 mediates brain development in mice (14). Akt1 (henceforth Akt) comprises three conserved domains: an N-terminal pleckstrin homology domain (PHD), a conserved catalytic kinase domain, and a flexible C-terminal regulatory domain (Fig. 1), which encompasses a phosphorylation site (15,16). Akt serves as a major component of the phospholipid signaling pathway involving

Submitted July 16, 2020, and accepted for publication March 18, 2021.
*Correspondence: nussinor@mail.nih.gov or agursoy@ku.edu.tr
Editor: Madan Babu.
https://doi.org/10.1016/j.bpj.2021.03.018

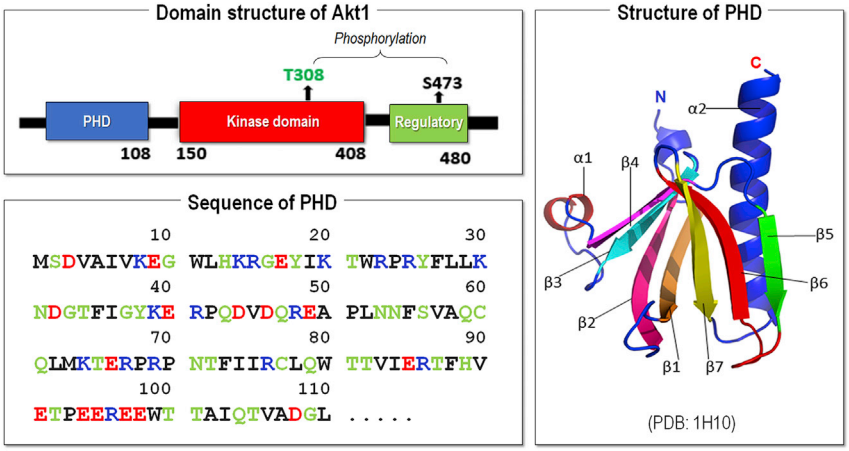

FIGURE 1 The domain structure of Akt and sequence and three-dimensional structure of the Akt PHD. In the domain structure of Akt (*upper left panel*), two phosphorylation sites (T308 and S473) are marked. In the sequence of the Akt PHD (*lower left panel*), the hydrophobic, hydrophilic/glycine, positively charged, and negatively charged residues are colored black, green, blue, and red, respectively. The crystal structure of the PHD of Akt (PBD: 1H10) with marked secondary structure (*right panel*) is shown. To see this figure in color, go online.

phosphatidylinositol 3,4,5-triphosphate (PIP_3). In this pathway, PIP_3 levels are controlled by the opposing actions of phosphatidylinositol 3-kinase (PI3K) and phosphatase and tensin homolog (PTEN) (17). The activation of Akt is instigated upon growth factor stimulation of PI3K, which leads to a higher concentration of PIP_3 at the plasma membrane from phosphatidylinositol 3,4-bisphosphate (PIP_2) (18–22). PIP_3 and PIP_2 phospholipids are localized in the plasma membrane, and PIP_3 binding to Akt's N-terminal PHD triggers its conformational change at the plasma membrane (3,18,22–24). Unlike most AGC kinases, which lack the PHD, the Akt PHD shows a high binding affinity for PIP_3 (25,26). The interaction of Akt's PHD and PIP_3 is a hallmark in Akt pathways and required for phosphorylation and downstream activation of effector proteins (19,23).

The PHD consists of a C-terminal amphipathic helix, two antiparallel sheets, and three variable loops (Fig. 1). Translocation of Akt to plasma membrane containing PIP_3 is required for its phosphorylation and activation, whereas Akt dissociation from the plasma membrane leads to rapid dephosphorylation and inactivation (27). Recruitment of Akt to the membrane (28) by CaM releases the autoinhibition of the kinase domain. Phosphorylation of Ser473 in the C-terminal regulatory domain by mammalian target of rapamycin complex 2 (mTORC2) and Thr308 at the activation loop in the kinase domain by phosphoinositide-dependent kinase 1 (PDK1) activate Akt (29,30). At the plasma membrane, Akt is regulated by phosphatidylserine (PS), where PS interacts with key residues in the PHD and regulatory domain, with the interaction promoting the binding of Akt to PIP_3 (31,32). The cooperativity between PS and PIP_3 was proposed to trigger Akt interdomain conformational changes leading to phosphorylation of Ser473 and Thr308 (31,32). In the absence of incoming signals, Akt is autoinhibited (27), with the PHD interacting with the kinase domain in a closed conformation (33,34), blocking phosphorylation of Thr308 by PDK1 (34). Relieving the autoinhibition upon PHD binding to CaM, and subsequently at the membrane to PIP_3 releasing CaM, exposes Thr308 for phosphorylation (33,35). Mutations in the PHD that weaken the interaction between the PHD and the kinase domain result in constitutive activation (36).

In breast cancer cells, calmodulin (CaM) binds to Akt (36). Upon epidermal growth factor simulation, CaM colocalizes with the PHD to the plasma membrane to enable Akt membrane binding and activation (4). Disruption of the interaction between CaM and the PHD by a CaM antagonist inhibited CaM-PHD translocation to the plasma membrane, leading to cell death in tumorigenic mammary carcinoma cells (4,37). Protein ligation studies established that binding of the PHD to the kinase domain linker promotes pSer473-Akt phosphorylation releasing the autoinhibition exerted by the PHD. According to one recently proposed mechanism, phosphorylation of Ser477/Thr479 activated Akt through an allosteric mechanism involving loop interaction with the kinase domain linker, which reduces PHD autoinhibition, lowering PIP_3 affinity (29). Taken together, these findings imply that synergies between membrane lipids and the PHD, interactions between the PHD and the kinase domain linker, and interactions between CaM and the PHD are required for Akt translocation, phosphorylation, and activation, respectively.

Akt is a critical node in the Ras/PI3K/Akt/mTOR pathway. Within our long-term aim of unraveling the activation and signaling of Ras oncogenic signaling and its dysregulation in cancer, recently, we deciphered the mechanism of PI3Kα activation at the atomistic level (38) and the structural basis for the role of Ras in the activation (39). Here, we take the next step in this pathway. NMR experiments established how CaM binds the PHD and showed the conformational changes that are involved, which facilitate translocating Akt to the plasma membrane. Here, employing atomistic molecular dynamics (MD) simulations, we explore the interplay between CaM and the Akt PHD that leads to Akt membrane anchoring and activation and, via PIP_3, to its release. To delineate how CaM releases the PHD at the membrane, we employed a small molecule, inositol 1,3,4,5-tetrakisphospahte (IP_4), the polar head of PIP_3, in the CaM-PHD interaction. The binding affinity of PIP_3 to Akt is greater than IP_4 (40). Our observations clarify

the activation mechanism, which may help in the discovery of Akt1-specific small molecules to inhibit this kinase. Nonspecific drugs that inhibit other Akt isoforms, for example, Akt2 in glucose metabolism, could result in a diabetes-like syndrome (41). Drugs targeting the interaction explored here may explore ATP noncompetitive allosteric drug away from the catalytic site.

MATERIALS AND METHODS

Generating initial configurations of CaM-PHD complex

Crystal structures of CaM with extended (PDB: 1CLL) and collapsed (PDB: 1CDL) linkers and the PHD of Akt (PDB: 1H10) bound to IP_4 were downloaded from the Protein Data Bank (PDB) (42). To obtain initial complex structures of CaM-PHD for MD simulations, the structures were docked using InteractiveROSETTA (43). Before docking, the missing NH_3 terminus and residues 1–4 of CaM were added using Discovery Studio (44). To collect multiple decoys, a series of docking were performed. The chemical shift perturbations (CSPs) from previous NMR studies (23,31) were traced, and highly perturbed residues (>0.1 ppm) were mapped on the crystal structures of CaM and the Akt PHD (Fig. S1). The mapped CSPs were used to guide the selection of the interface residues. The predicted CaM-PHD complex decoys were ranked based on the Rosetta scoring energy function. We meticulously selected the CaM-PHD dimeric complexes based on these scores, conformations, and interface residues that were in agreement with the NMR data (23,31). For every CaM conformation, initial configurations of the CaM-PHD complex were selected: five configurations (Configs. 1–5) with the extended CaM and three configurations (Configs. 6–8) with the collapsed CaM. Using NACCESS software (45), the accessible surface areas for all configurations (Configs. 1–8) (Table S1) were calculated. The docking results from InteractiveROSETTA (43) showed that the N-lobe of CaM with the extended linker alone is incapable of Akt-PHD binding, but the C-lobe alone is. The prediction tool, Protein Interactions by Structural Matching (46), gave similar binding modes between CaM and the Akt PHD. IP_4 is the polar head of PIP_3, whereas IP_3 is the polar head of PIP_2. Both molecules (IP_4 and IP_3) lack the acyl chains and/or the glycerol group, which is essential for lipid binding. Of note, during the docking, IP_4 was excluded or removed from the PHD to generate only CaM-PHD complexes. To observe the effect of IP_4 on the CaM-PHD interaction, initial configurations of the CaM-PHD complex containing IP_4 by adding IP_4 to the β-sandwich pocket of the PHD using the same configurations (Configs. 1–8) were generated by PyMOL molecular graphics system (47). Eight additional configurations with IP_4 were obtained: five configurations (Configs. 9–13) with the extended CaM and three configurations (Configs. 14–16) with the collapsed CaM (Table S2). The CHARMM all-atom additive force field (version c42) (48,49) was employed to build all simulation inputs. In the simulations with the small molecules IP_3/IP_4, the coordinates of 4IP (IP_4 in this study) were extracted from the crystal structures of the Akt PHD (PDB: 1UNQ and 1H10). The standard CHARMM program (48) provides the topologies and parameters for the phosphatidylinositol lipids, PIP_2 and PIP_3. The inositol headgroups of the lipids were extracted and modified to IP_3 and IP_4. The same topologies and parameters adopted from the phosphatidylinositol lipids were applied to these small molecules.

Atomistic MD simulation protocol

After the docking, we performed atomistic MD simulations for all 16 configurations with and without IP_4 in solution. These simulations closely mirrored the protocol described in our previous publications (50–60). Several rigid body minimization steps (10,000 steps) followed by a dynamic cycle of 50,000 steps for all systems were implemented. The TIP3P water model was utilized to generate the isometric unit cell box, which contains the protein complex. The unit cell box dimensions are $100 \times 100 \times 100$ Å^3, containing 265 protein residues in total with 148 residues in CaM and 117 residues in the Akt PHD. Subsequently, the systems were neutralized with counterions and satisfied a total ion concentration near 100 mM: 68 Na^+ and 50 Cl^- (complexes without IP_4) and 72 Na^+ and 46 Cl^- (complexes with IP_4). We applied harmonic restraints to all heavy atoms ($k = 5$ kcal/mol/Å^2/atom) and gradually relaxed to $k = 0$ with a full particle mesh Ewald calculation for long-range electrostatic interactions in the pre-equilibration stages of the simulations. Also, a 12 Å cutoff local interaction distance was used for both the electrostatic and van der Waals (vdW) calculations and a scaling factor for one to four short range electrostatic and vdW interactions. Next, the Langevin temperature control was employed to maintain a constant temperature at 310 K. Nosé-Hoover Langevin piston pressure control was used to sustain the pressure at 101,325 Pa (1 atm). For production runs of 1 μs (1000 ns) at 2 fs/step, the NAMD parallel-computing code (61) was employed on the Biowulf cluster at the National Institute of Health (Bethesda, MD). To guarantee that equilibrium was reached for each system, the root mean-square deviation (RMSD) and energy trajectories were computed as a function of time. Finally, we deploy the CHARMM program (48) to analyze the simulation trajectories. Averages were taken after 300 ns, discarding initial transient trajectories. The average interaction energy was calculated over the last half of the 1 μs trajectory, ensuring that the systems reached to equilibration after 500 ns. The presented total interaction energy calculated by the CHARMM program (48) is a sum of electrostatic and vdW interactions between two proteins.

Binding free energy calculation of the CaM-PHD complex

To determine the binding free energy of the CaM interaction with the Akt PHD, we used the molecular mechanics energies combined with the generalized Born surface area continuum solvation (MM-GBSA). As shown in Eq. 1, the average binding free energy constitutes three components: the gas phase contribution, the solvation contribution, and the entropic contribution,

$$\langle \Delta G_b \rangle = \langle \Delta G_{sol} \rangle + \langle \Delta G_{gas} \rangle - T\Delta S, \quad (1)$$

where the notations G_b, G_{sol}, G_{gas}, and $T\Delta S$ denote the binding free energy, the solvation energy contribution, the gas phase contribution, and the entropic contribution respectively, and the angle brackets indicate the average along the simulations. The solvation free energy was calculated by the GB using the GBSW module (62) of the CHARMM program (48). The total entropy term in Eq. 1 above is further partitioned into the translational, rotational, and vibrational contributions. We evaluated the translational and rotational entropies from the calculation of principal moment of inertia and obtained the vibrational entropy from the quasiharmonic mode calculation in the VIBRAN module of the CHARMM program (48). The alteration in binding free energy due to the complex formation between CaM and the Akt PHD is computed as follows:

$$\Delta G_b = G_b^{Complex} - \left(G_b^{CaM} + G_b^{PHD}\right). \quad (2)$$

The full description of the calculation protocol has been published elsewhere (51–60). The change in binding free energy triggered by the presence of IP_4 in the CaM-PHD interaction can be obtained by the calculation

$$\Delta\Delta G_b = \Delta G_b^{with} - \Delta G_b^{without}, \quad (3)$$

where "with" and "without" denote involvement of IP_4 in the CaM-PHD interaction.

Clustering the ensembles

Ensemble Cluster in Chimera (63) can cluster members of a conformational ensemble of a protein containing the same atoms and present the clusters of protein conformations. To determine the most populated (favorable) state (conformation) of each CaM-PHD dimeric complex, we clustered all the simulation frames using Chimera (63) with a step size of 10 and selected the topmost clusters. The ensemble clustering in Chimera is based on pairwise best-fit RMSD values, which returns the clusters, their sizes, and their conformational representatives. In the clustering, 10,000 frames for each configuration from the simulations were employed in Ensemble Cluster using a tool in the MD/Ensemble Analysis categories. Bio-3D (64) was deployed to perform principal component analysis (PCA) on the trajectories for each model to obtain a PCA conformer plot, a scree plot, and a collective motion defined by PC1.

RESULTS

Atomistic MD simulations were carried out on the 16 configurations of CaM-PHD complexes. Configs. 1–8 are without IP_4 (Fig. S2 *A*) and Configs. 9–16 with IP_4 (Fig. S2 *B*). During the simulations, the interaction between CaM and the Akt PHD appears to be thermodynamically stable, favorable especially for configurations with extended CaM as depicted in the final conformations of the CaM-PHD complex (Fig. 2 *A*). However, when IP_4 is loaded onto PHD (Fig. 2 *B*), the CaM-PHD interaction appears weaker, causing the N-lobe of CaM to rapidly dissociate from the complex. In the collapsed form of CaM, some configurations show stronger binding in the presence of IP_4, especially when IP_4 is far away from the CaM-PHD interface. The RMSD profiles (Fig. S3) of the configurations show that the PHD is more stable compared to CaM, whose fluctuation increases when IP_4 was involved in the dimeric interface.

Selection of best models for the CaM-PHD dimeric complex

After the simulations of selected models, statistical and conformational analyses were performed to select the best would-be models of CaM-PHD dimeric complexes. First, we computed the total interaction energy (contributions from electrostatic and vdW interactions) for the complex with and without IP_4. For Configs. 1–8 without IP_4 (Fig. S4 *A*), the averaged total interaction energy showed that the extended CaM (Configs. 1–5) appears to have a stronger interaction with Akt-PHD than the collapsed CaM (Configs. 6–8), suggesting a favorable CaM conformation in the interaction with the PHD. It is expected that in the presence of IP_4, the interaction of CaM with the Akt PHD can decrease because of competition with IP_4. This prompts us to delineate probable models of the CaM-PHD interaction. For CaM with the extended linker, Configs. 9, 11, and 13 decrease the CaM-PHD interaction when IP_4 is loaded to the PHD compared with the corresponding Configs. 1, 3, and 5 without IP_4, respectively (Fig. S4 *B*). This is consistent with experimental findings (23) when CaM cannot extract the Akt PHD from the plasma membrane. The experimental results showed that the Akt PHD has a greater affinity to PIP_3-containing membranes and CaM is displaced and unable to bind concomitantly (23). However, Configs. 10 and 12 with IP_4 increase the CaM-PHD interaction compared with the corresponding Configs. 2 and 4 without IP_4, respectively, indicating a less favorable model of the CaM-PHD interaction. For CaM with the collapsed linker, we also observed that Configs. 14–16 with IP_4 increase the CaM-PHD interaction compared to Configs. 6–8 without IP_4, respectively. This suggests that the collapsed CaM may not be a populated conformation in the interaction with the PHD.

Next, we determined the Gibbs free energy from MM-GBSA calculations (Fig. 3). The details of the decomposition of each term of the Gibbs free energy are summarized in Table S3. The MM-GBSA results were largely consistent with the interaction energy. Configs.1, 2, 5, 3, and 4 are arranged in the order of decreasing binding free energy, all of which agreed with the NMR data (23,31) except Config. 4. That is, Config. 12 with IP_4 has a more favorable binding free energy than Config. 4, which contradicts the experimental findings (23). Also, the MM-GBSA results indicate that the CaM with collapsed linker is not consistent with NMR experiments. For instance, Configs. 6 and 7 without IP_4 yielded positive values of the binding free energy, whereas Configs. 14 and 15 with IP_4 yielded negative values of the binding free energy. Config. 8 without IP_4 yielded negative binding free energy, but Config. 16 with IP_4 shows a better binding. Finally, we computed the change in binding free energy, $\Delta\Delta G_b$, due to the presence of IP_4 for all systems (Table 1). $\Delta\Delta G_b$ is increased for Configs. 1, 2, 3, and 5, indicating that IP_4 possibly disrupts or weakens the interaction between CaM-PHD, consistent with the experiments. For the remaining configurations, we observed what was contrary to the NMR experiments (23,31). In short, Configs. 1, 2, 3, and 5 of CaM-PHD complexes were selected as our best models based on our criteria, which are supported by the NMR data (23,31). Our modeling suggests that the extended CaM may be the populated conformation in the interaction with the PHD.

Interface residues of CaM-PHD dimeric complexes

NMR, as well as other biophysical and biochemical methods, has unearthed CaM's binding to the Akt PHD with a dissociation constant (K_d) of 100 nM in a 1:1 stoichiometry (23). These experiments have also revealed that CaM's N- and C-terminal lobes are essential for Akt-PHD binding and that electrostatic interactions greatly contribute to CaM-PHD association. Moreover, favorable hydrophobic interactions appear to stabilize the CaM-PHD dimeric complex (23). After the MD simulations, the types of

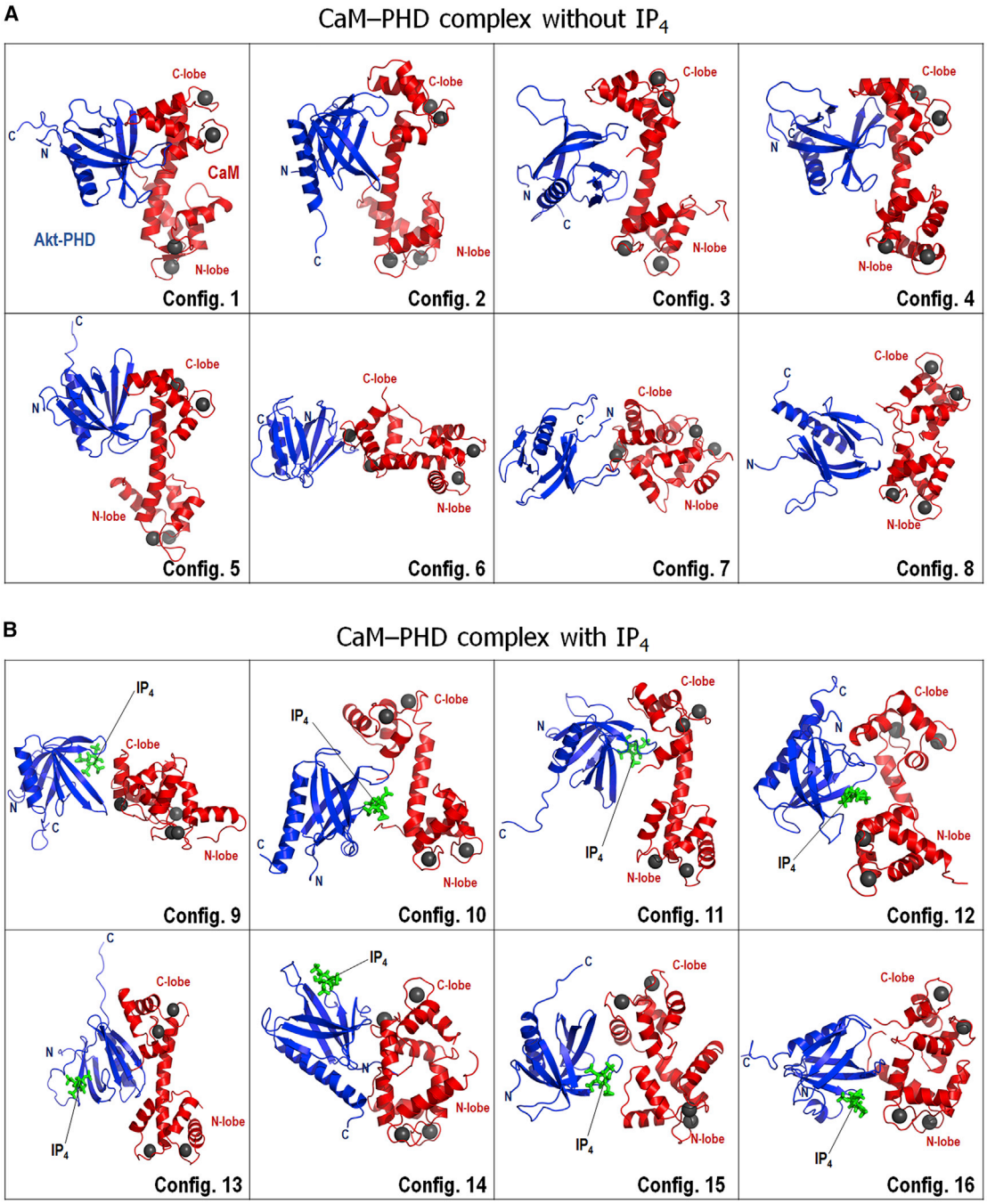

FIGURE 2 Final structures of the CaM-PHD complex. Cartoon representatives of the CaM-PHD complex for (*A*) Configs. 1–8 without IP_4 and (*B*) Configs. 9–16 with IP_4 are shown. CaM is colored red, and the PHD is colored blue. The N-lobe and C-lobe of CaM are marked. The marked "N" and "C" denote the N- and C-terminus of PHD, respectively. A small molecule, IP_4, in the pocket of the PHD is marked. To see this figure in color, go online.

intermolecular interactions (salt bridge, nonpolar, and H-bond) in CaM-PHD complexes throughout the MD trajectories (Tables S4 and S5) were analyzed for all configurations. Here, the residue pairs are treated as interface residues and considered effective and counted if they have at least 50% occurrence. To corroborate the CaM-PHD dimeric interface, we examined important residues involved in the dimeric complex. For instance, in Config. 1, salt bridge formation between residues R74-E85, D58-R67, E114-K14, E114-R25, E120-R25, E123-R23, K77-E85, D2-R76, E84-R76, and E120-R23 (where the former and latter residues denote CaM and PHD, respectively) retains the dimeric interface. Also, nonpolar interactions between residues I9-M63, A73-M63, M124-I19, A128-I19,

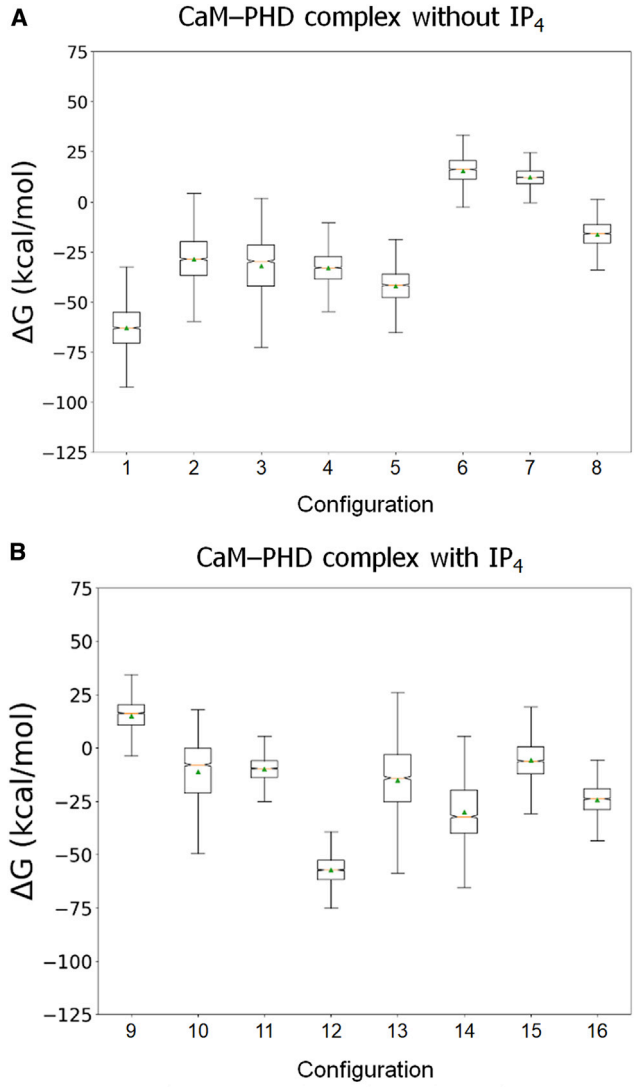

FIGURE 3 Binding affinity of CaM-PHD. Using Matplotlib in Python, the binding free energy for the CaM interaction with the Akt PHD during the simulation for (*A*) Configs. 1–8 without IP_4 and (*B*) Configs. 9–16 with IP_4 has been plotted. In the box graphs, the triangle symbol and horizontal line indicate the mean and median values, respectively, and the box plots and error bars represent the percentage and the standard deviation, respectively. To see this figure in color, go online.

M144-I19, L112-I84, F92-I84, G113-F55, M71-P68, and L4-M63 contributed to the complex formation. Polar interactions between residues T5-Q61, T70-T65, Q143-Y18, and Q3-Q61 and a hydrogen bond between A128-Y18 appear to strongly contribute to the CaM-PHD association. Similar analyses were performed for the remaining complexes. In Config. 4, although both salt-bridge and nonpolar interactions contribute to the binding, we observe no polar interactions and H-bond formations between CaM and the PHD, which may have led to a decrease in the overall binding strength. For the collapsed CaM without IP_4 (Configs. 6, 7, and 8), salt bridges and nonpolar and polar interactions contribute to the binding energy. H-bonds are observed in

TABLE 1 The change in binding free energy, $\Delta\Delta G_b$, due to the presence of IP_4 in the CaM-PHD interaction

CaM-PHD complex with IP_4		CaM-PHD complex without IP_4		
Config.	ΔG_b (kcal/mol)	Config.	ΔG_b (kcal/mol)	$\Delta\Delta G_b$ (kcal/mol)
9	13.66	1	−57.46	71.13
10	−8.73	2	−39.37	30.63
11	−6.19	3	−33.44	27.24
12	−47.46	4	−23.58	−23.88
13	−4.38	5	−37.14	32.76
14	−32.77	6	10.83	−43.61
15	−5.78	7	10.25	−16.04
16	−19.74	8	−16.53	−3.21

Binding free energy calculated by Eq. 3.

Configs. 6 and 8, but not Config. 7. It came as no surprise that in Config. 9 (IP_4 form of Config. 1) with fewer H-bonds, nonpolar and polar interactions and salt bridges are lost, suggesting that IP_4 contributed to weakening the interaction. Further still, in Configs. 10 and 11, salt bridges and nonpolar interactions occur. Polar interactions are observed in Config. 10, but not in Config. 11, and both contain no H-bonds, also indicating that IP_4 disrupted the interaction. For Configs. 12 and 13, there is no loss of salt bridges, H-bonds, and nonpolar and polar interactions; however, in Config. 12, although polar interactions and H-bonds occur, these interactions are lost in Config. 4. Finally, Configs. 14, 15, and 16 retain a greater number of salt bridges, H-bonds, and nonpolar and polar interactions compared with Configs. 6, 7, and 8, respectively, hence decreasing their binding free energies. This decrease in binding free energy between the collapsed CaM and PHD suggests that IP_4 plays an infinitesimal role in disrupting the interactions but may contribute to the binding energy. This observation was also not surprising because the binding pocket of IP_4 in the PHD is oriented differently from the binding region of the collapsed CaM. Taken together, we hypothesize that IP_4 can weaken the interaction between the extended CaM-PHD complex, whereas IP_4 is unlikely to disrupt the interaction between a collapsed CaM-PHD complex.

Some common salt bridges were found in the following pairs of configurations: Config. 1 and Config. 2 (E114-R23), Config. 1 and Config. 3 (R74-E85, E123-R23, E120-R23), and Config. 1 and Config. 5 (E114-K14, E114-R25). Interestingly, no common salt bridges were found among the complexes, which may be attributed to different conformations of predicted docked structures. Additionally, comparing the complex without IP_4 and with IP_4 pairs (Tables S4 and S5), we observed the following: for Config. 1, there are 10 salt bridges, all of which are lost in Config. 9; for Config. 2, there are three salt bridges, whereas in Config. 10, there are two salt bridges, and no common salt bridges were found between them. In Config. 3 and Config. 11, three common salt bridges are found (K115-E40, E114-R25, and E127-R69), and there are nine

salt bridges in Config. 3 compared with Config. 11, which has four salt bridges.

To what extent do the interface residues of CaM-PHD complexes correspond to the NMR chemical shift data?

We observed a significant number of residues that correlate with the experimental NMR data observations (23,31). For instance, upon titration of CaM's N-lobe into Akt-PHD, residues R16, I19, T21, V45, N53, T82, I103, T105, V106, D108, K111, T82, and W80 in the PHD showed large chemical shift changes. Titration of CaM's C-lobe into the Akt PHD led to noticeable chemical shift changes for residues including K14, R15, G16, I19, T21, W22, R23, V45, E49, and N53. To complement the NMR CSPs, we calculated the backbone amide CSPs for the PHD residues using the SHIFTX2 program (61). The program uses the protein coordinates as input to predict the backbone and side-chain ^{1}H, ^{13}C, and ^{15}N chemical shifts for proteins. The best representative models of the CaM-PHD complex, Configs. 1, 2, 3, and 5, were subject to the CSP calculations. In the PHD, many residues exhibit perturbations upon binding to CaM (Fig. 4). Among the residues with >0.1 ppm, R15, G16, Y26, G37, D44, V45, Q59, and W80 significantly contribute to the interaction with CaM, consistent with the NMR CSPs. Also, in CaM, hydrophobic residues or the methyl group (CH_3) of Met, M36, M51, M71, M72, M76, M109, M124, M144, and M145 located in the C-terminal lobe within the hydrophobic patch contributed to Akt-PHD binding. The NMR experiments also affirmed that the Akt PHD engages both lobes of CaM, with CaM's N-lobe recognizing the loop connecting β6 and β7, whereas the C-lobe tends to bind to the loop connecting β1 and β2 (31). Assessing our predicted complex for the occurrence of these residues in the interfaces, several residues were found within the interfaces that agreed with the NMR data (23,31) (see Tables S4 and S5). For example, in Config. 1, we found salt bridge formation between the residues E114-K14, E114-R25, and E84-R76; nonpolar interactions between the residue pairs M124-I19, M144-I19, and M71-P68; and an H-bond between A128 and Y18. Similarly, for Config. 3, we also observe nonpolar interactions between the following pairs of residues: M109-I19, M144-I19, M145-I19, M72-W80, M76-W80, and F92-I19. Altogether, the occurrence of these residues in the interfaces of the predicted complexes confirms our predicted models. Correspondingly, I19 and Y18 in the Akt PHD were greatly involved in nonpolar and polar interactions, respectively. The involvements of I19 and Y18 in these atomic interactions were unsurprising because they are located within the loop connecting β1 and β2. The aromatic residue W80, located in the loop connecting β6 and β7, was significantly involved in nonpolar interactions with several CaM residues, M71, M51, and L69. An aromatic residue like Trp has a high tendency to anchor to hydrophobic regions of CaM. Taken together, these analyses showed that Configs. 1, 2, 3, and 5 are especially good models for further studies to elucidate the association between CaM and the PHD.

In a similar vein, we identified and mapped the interface residues of our best complex model using the best representative structures from the MD simulations. The goal was to evaluate the selected complex configurations and determine their agreements with the NMR data (23,31). Snapshots representing the conformations of the best configurations of CaM-PHD dimeric complexes (Configs. 1, 2, 3, and 5) without IP_4 are illustrated in Fig. 5. We use our HotPoint server (66) to extract these interface residues. Consistent with the NMR data, for Config. 1, we again observe the occurrence of the residues K14, R15, E17, Y18, I19, K20, R23, and R25 at the Akt PHD interface, whereas in CaM, M71, E114, M124, M144, M145, and A147 also occur at the interface (Table 2). The occurrence of CSP residues from the NMR experiments is observed in the remaining configurations. We observed that the β-sheets in the Akt PHD, especially β1, β2, β6, and β7, and the loops that connect them are significantly involved in binding CaM, whereas the N- and C-terminal lobes and the central linker of CaM are required for Akt-PHD binding. Taken together, the MD simulations indicate that the binding of CaM to the Akt PHD is thermodynamically stable but differs from CaM's typical binding mode, which usually involves helical regions (67,68).

Clustering CaM-PHD dimeric complexes

Using Chimera (60), the ensembles of the CaM-PHD complex conformation were clustered. For Config. 1, the top cluster 1 contains 2070 members, which corresponds to a probability, $p = 0.21$ (21%), that is 2070 out of the total 10,000 frames. Also, for Configs. 2, 3, and 5 in cluster 1, there were 1380, 2050, and 980 members corresponding to 14, 21, and 10%, respectively. The structures for each configuration's best-approximated representative clusters for Configs. 1, 2, 3, and 5, which were selected as our best models based on our criteria, are presented in Fig. 6. For a comparison purpose, we also collected the structures for the other models, Configs. 4, 6, 7, and 8, in Fig. S5. Based on the information obtained from the clustering coupled with conformational analyses, we propose and present the favorable configurations for CaM binding to the Akt PHD. We deduce that both the N-lobe and C-lobe, as well as the central linker of CaM, are vital for Akt-PHD binding. However, although the tightly bound C-lobe and the central linker of CaM may be enough for Akt-PHD binding, the N-lobe alone is not enough, with the weak binding rapidly dissociating when IP_4 is loaded onto the PHD. To observe the conformational changes for configurations with and without IP_4, we aligned the top two cluster representatives for selected models (Configs. 1, 2, 3, and 5) (Fig. S6). We

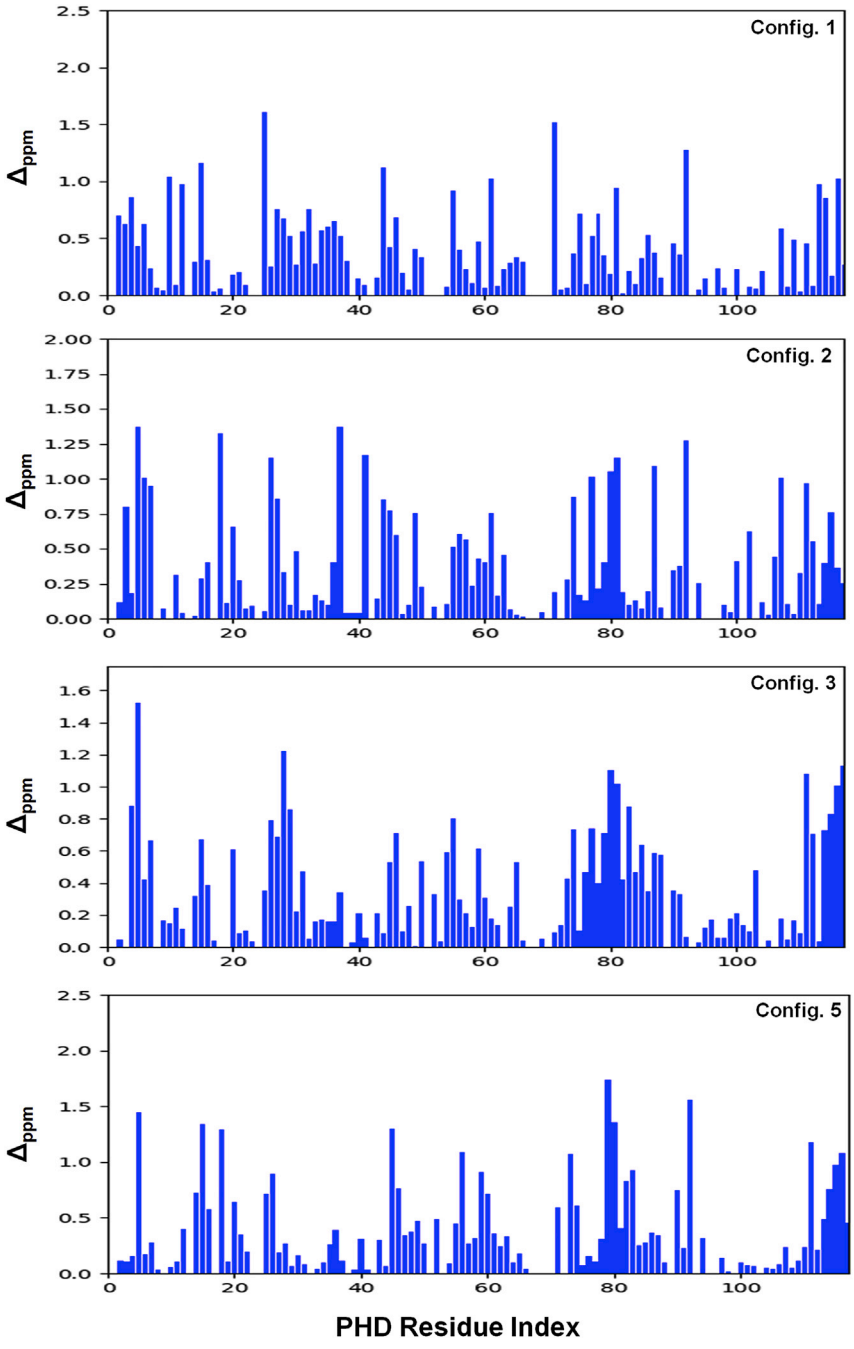

FIGURE 4 The calculated amide CSPs for the PHD residues in the CaM-PHD configurations (Configs. 1, 2, 3, and 5). The ^{1}H, ^{13}C, and ^{15}N chemical shifts were computed by the SHIFTX2 program (65). The combined CSPs for the PHD over the CaM-PHD complex trajectory and the PHD alone trajectory were computed during the MD simulations utilizing the equation $\Delta_{ppm} = \sqrt{(\Delta\delta_{HN})^2 + (\Delta\delta_N \alpha_N)^2}$, where δ_{HN} and δ_N indicate the ^{1}H and ^{15}N chemical shift difference, in the order given between the CaM-PHD and the PHD trajectories. A scaling factor, $\alpha_N = 0.17$, was applied to the difference in ^{15}N chemical shift. To see this figure in color, go online.

observed significant conformational rearrangements of CaM in the complex due to the presence of IP_4 in the PHD.

PCA of CaM-PHD dimeric complexes

Deploying Bio-3D (64), an R package for comparative analysis of protein structures, the PCA plots were obtained for all models using the simulation trajectories. PCA is a widely established multivariate method utilized to reduce the number of dimensions that are required to describe the dynamics of protein via a decomposition process that filters observed dynamics from the largest to the smallest spatial scales (69). PCA extracts the most essential elements in the data by using a covariance matrix or a correlation matrix (hereafter called C-matrix) constructed from atomic coordinates that describe the protein's accessible degree of freedom, such as the Cartesian coordinates that define atomic displacements in each conformation in the trajectory (70). Additionally, an eigenvalue decomposition of the C-matrix usually results in a complete set of orthogonal collective modes (eigenvectors), where each eigenvector constitutes a corresponding eigenvalue (variance), which characterizes a

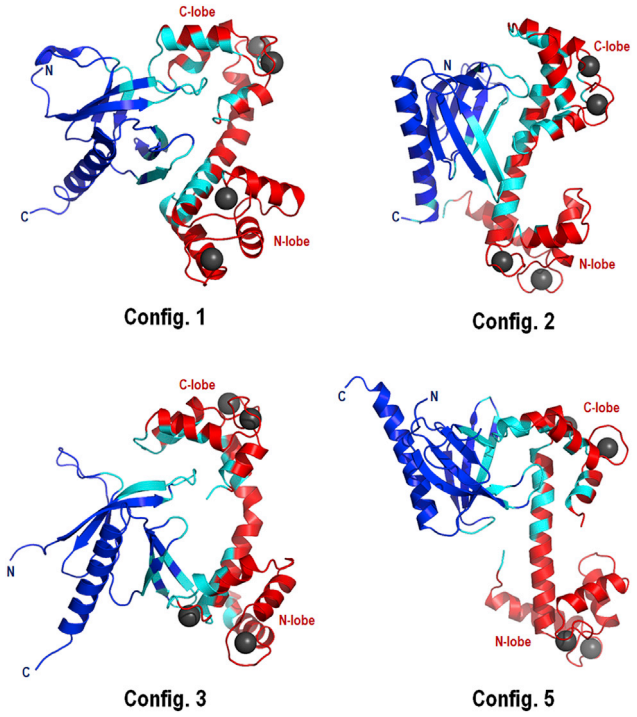

FIGURE 5 The best conformations of the CaM-PHD complex. Snapshots representing the best conformations of the CaM-PHD complex—Configs. 1, 2, 3, and 5, without IP_4—are given. In the solid ribbon presentation of the secondary structure, the PHD and CaM are colored light blue and red, respectively. Ca^{2+} is colored gray and depicted as a sphere. The interface residues between the CaM and PHD are colored cyan and listed in Table 2. To see this figure in color, go online.

portion of the motion, where larger eigenvalues describe motions on larger spatial scales (71). For protein structural analysis, PCA transforms atomic coordinates into a few PCs (usually two or three) that represent directions where the structure set displays the largest collective variances. Of principal importance, PCA generates a conformer plot that permits interpreting interconformer relationships. Also, a scree plot, which displays the eigenvalues arranged in descending order, can be utilized to determine significant PCs that capture domain collective variances in the structure set. PCA also outputs a representation of the collective structure motions captured by the top PCs, which are often related to the protein function (72). The PCA examines the relationship between the various conformations sampled over a subset of the trajectory of 500–1000 ns (6000 frames) using the Cα atoms of all models of CaM-PHD complexes (265 Cα atoms) without IP_4 (Figs. 7 and S7). Using hierarchical clustering in Bio-3D (64), we generated the PC1 vs. PC2 conformer plot, scree plot, and the collective motion defined by PC1 for all models without IP_4 to depict important variations or conformational changes in the CaM-PHD dimeric complex. For the best models (Configs. 1, 2, 3, and 5), the PC1 vs. PC2 conformer plot of Config. 1 account for over 46% of the variance; likewise, Config. 2, 3, and 5 plots account for over 59, 43, and 45% of the variance, respectively (Fig. 7). Similarly, for the less favorable models, the PC1 vs. PC2 plots of Configs. 4, 6, 7, and 8 account for over 57, 62, 79, and 48%, respectively (Fig. S7), with Config. 7 capturing most of the variation or essential dynamics. The scree plots showed the eigenvalues arranged in descending order for all models. For instance, the eigenvalues of the scree plot for Config. 1 descended from 89.2 to 36.5. The collective motion defined by PC1 presented the CaM-PHD complex structure colored by the *B*-factor, representing the similar ensembles of the conformations as observed in cluster 1 by Chimera. These conformer plots, scree plots, and collective motions defined by PC1 for all eight models that were sampled throughout the simulations succinctly uncovered important conformational variations or essential dynamics for CaM-PHD dimer association.

DISCUSSION

Activation of Akt, the paradigmatic lipid-activated kinase, is crucial for modulating apoptosis, cell proliferation, and oncogenesis. Akt activation is a fairly common tumorigenic occurrence in many cancer types such as breast cancer

TABLE 2 Interface reside of top must cluster of the best models, Configs. 1, 2, 3, and 5

CaM-PHD complex	CaM	PHD
Config. 1	L4, T5, E6, Q8, I9, A57, E67, T70, M71, A73, M76, K77, L105, M109, L112, G113, E114, K115, L116, T117, E119, E120, E123, M124, E127, A128, V136, F141, M144, M145, A147, K148	K14, R15, G16, E17, Y18, I19, K20, T21, R23, R25, K39, P51, L52, N53, N54, Q61, M63, K64, T65, E66, R67, I74, R76, V83, I84, E85, R86, T87
Config. 2	A1, D2, M51, E54, V55, T70, M71, R74, K75, K77, D80, S81, E83, E84, E87, A88, V91, F192, I100, L105, V108, M109, L112, E114, L116, M124, I125, E127, A128, V136, F141, M144, M145, A147, K148	E17, Y18, I19, K20, T21, R23, T34, A50, P51, L52, N53, N54, F55, S56, A58, Q79, W80, T81, T82, V83, I84, E85, R86, Q113, E116
Config. 3	E7, I9, D50, N53, E54, V55, D56, A57, D58, G59, D64, F65, P66, E67, L69, T70, R74, I85, E87, A88, V91, F92, L105, V108, M109, L112, G113, E114, K115, L116, E120, M124, M144, M145, A147, K148	R15, E17, Y18, I19, K20, T21, W22, R23, P24, R25, K39, E40, Q61, L62, M63, T65, R67, P68, R69, I74, R76, L78, W80, T81, T82, V83, E85
Config. 5	A1, D2, D80, S81, E84, I85, E87, A88, V91, F92, K94, I100, L105, V108, M109, T110, N111, L112, G113, E114, K115, L116, M124, I125, A128, V136, F141, M144, M145	K14, R15, E17, Y18, I19, K20, W22, P51, L52, N53, N54, F55, P68, R69, P70, W80, T82, I84, E85, R86, T87

Of note, these interface residues were obtained within 4 Å distance.

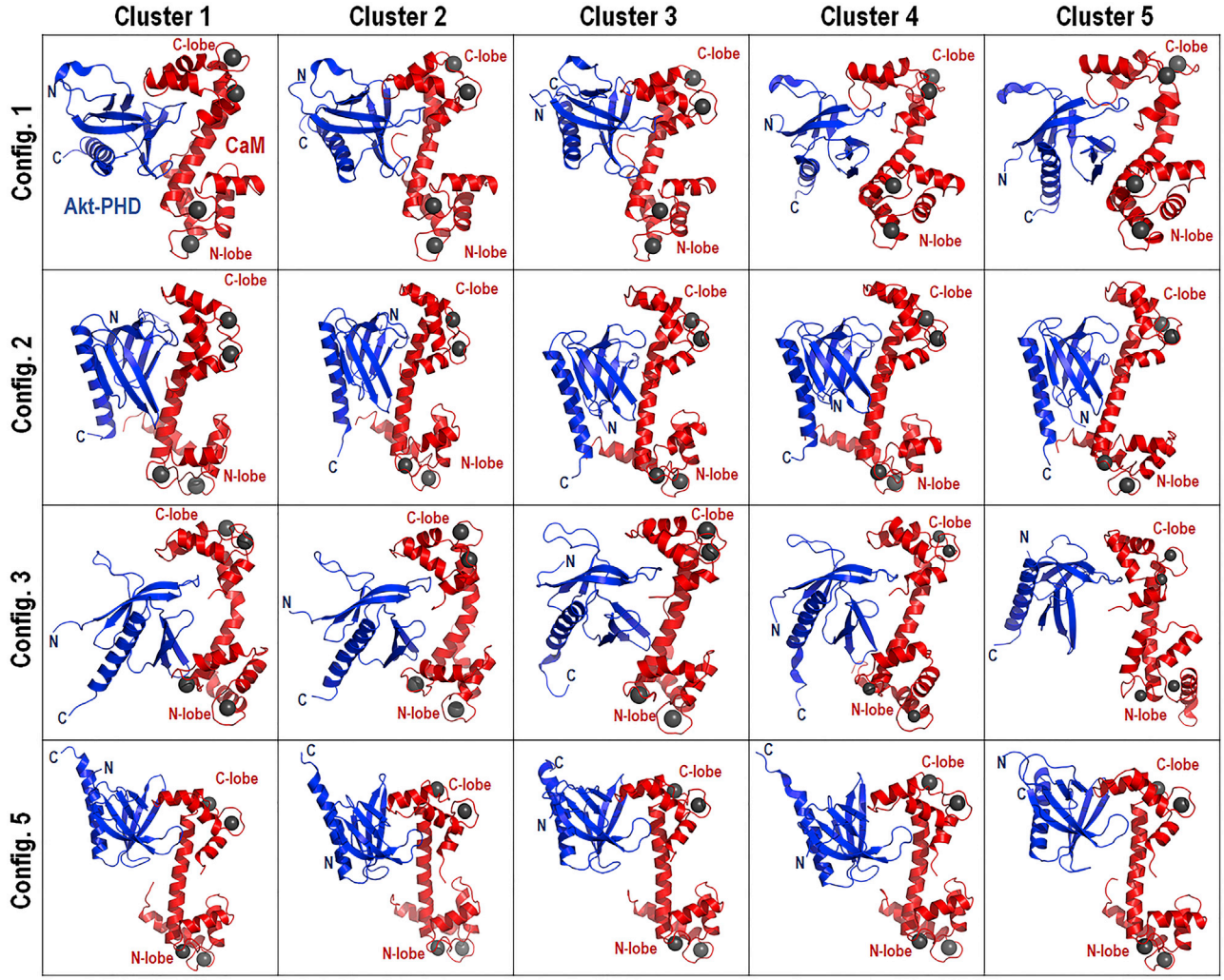

FIGURE 6 The best-approximated representative clusters of the CaM-PHD complex for Configs. 1, 2, 3, and 5. Conformation of the best-approximated representative clusters of each model. The top five cluster representatives of best model for Config. 1 were defined with probabilities $p = 0.21$, 0.18, 0.12, 0.10, and 0.08 for clusters 1–5, respectively. For Config. 2, $p = 0.14$, 0.10, 0.09, 0.07, and 0.06; for Config. 3, $p = 0.21$, 0.10, 0.09, 0.08, and 0.07; for Config. 5, $p = 0.10$, 0.09, 0.07, 0.61, and 0.06 for clusters 1–5, respectively. The ensemble clustering was based on pairwise best-fit RMSD values, which returns the clusters, their sizes, and their conformational representatives. To see this figure in color, go online.

(3,18,25). Like other AGC kinases, Akt possesses an N-terminal PHD, which shares similar structural features with hundreds of analogs in mammals and bacteria (73–75). The PHD of Akt plays a critical role in recruiting Akt to the plasma membrane for activation. The Akt PHD interacts with PIP_3, a small signaling phospholipid localized on the inner leaflet of the plasma membrane (3,18,24). Akt translocation to the plasma membrane—an event that triggers its subsequent phosphorylation and activation—was proposed to be regulated by PS (32) to promote binding of the Akt PHD to PIP_3. A study by Lucic et al. (27) suggested that Akt phosphorylation and activation by association with membrane lipids are mutually independent. The study further proposed that, in the absence of PIP_3 Akt is dephosphorylated—an event enhanced by interaction between its kinase domain and the PHD—an interaction that leads to Akt autoinhibition (27). Recent investigations have also suggested that pSer473-Akt activation may be driven by interplay between the PHD and kinase domain linker that relieves PHD-mediated Akt autoinhibition. In that proposed mechanism, twofold phosphorylation at Ser477/Thr479 activated Akt through allosteric mechanisms involving activation loop interaction, which relieves the autoinhibition by the PHD and weakens PIP_3 affinity (29). Finally, another proposed mechanism posited that Akt activation in breast cancer involves interaction between its PHD and the dumbbell-shaped CaM (4,37). Disruption of the CaM-PHD association by an Akt antagonist inhibited CaM-PHD recruitment to the plasma membrane and resulted in cell death in mammary carcinoma (4). Collectively, several mechanisms for Akt translocation to the plasma membrane and activation have been proposed. Here, we established via

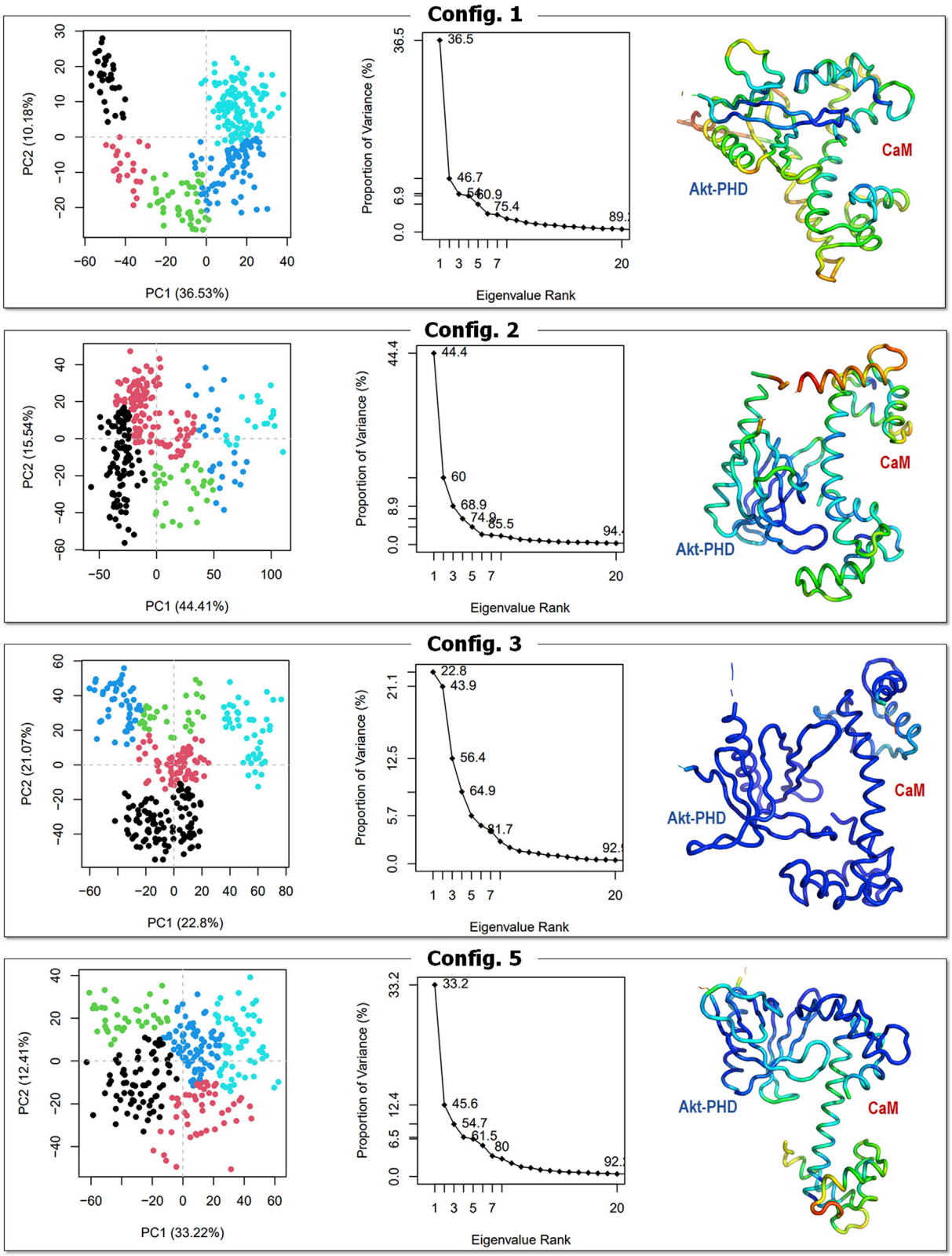

FIGURE 7 PCA for the best models. PC1 vs. PC2 conformer plot for Configs. 1, 2, 3, and 5 shows five distinct clusters obtained via hierarchical clustering (hc, $k = 5$, *left panels*), the eigenvalue scree plot (*middle panels*), and the collective motion for the CaM-PHD complex defined by PC1 representing the structure colored by *B*-factor or temperature factor (*right panels*). In the *B*-factor structure, blue and red denote atoms with low and high-temperature values, respectively, and light blue, white, and pink denote intermediate temperature values. To see this figure in color, go online.

MD simulations the detailed intermolecular interaction between CaM and the Akt PHD and the consequences of the IP_4 interaction, thereby clarifying the mechanism of recruitment to, and release at, the plasma membrane.

Calcium binding triggers conformational changes in CaM that expose hydrophobic residues enabling binding to cytosolic target proteins, including partners that are implicated in controlling cell shape and migration (76) and different targets (77). Computational modeling supported by NMR established that CaM uses its lobes for binding to the hypervariable region and the catalytic domain of K-Ras (78) and the cSH2 and nSH2 domains of p85α, the regulatory subunit of PI3Kα (79). In the Ca^{2+} bound state, electrostatics alters CaM conformational distributions and dynamics (80), and ensemble analyses with ClustENM (81) showed that CaM's C-lobe has greater mobility compared with the N-lobe. Genetic analysis and protein coprecipitation indicated that the CaM binding segment on Akt is within the first 42 residues (82), which forms a three-stranded β-sheet. CaM binding to the β-sheet is, however, rare because CaM binding fragments often populate α-helical regions (67,68). Usually, CaM binding segments on target proteins are ~15–20 residues, are hydrophobic/nonpolar with a basic character, and have a high tendency to form an α-helix (68,83). The NMR experiments (23,31), as well as our MD simulations, do not point to an α-helical region. The NMR data (23,31) and our simulations clearly showed that CaM interaction with the Akt PHD involves β-sheets and the loops that connect them. A similar binding mode has been observed for CaM and the Itk PHD. Itk (interleukin-2-inducible tyrosine kinase) belongs to the Tec kinase family (84). Also, a more recent study that aimed to investigate the direct interaction between CaM and the growth receptor bond 7 (Grb7) protein showed that CaM interacts with the PHD of Grb7 (85). There, CaM's peculiar binding motif was mapped to the β-sheet and not an α-helical region (85). The NMR CSP data for the Akt PHD indicated that it interacts with CaM via the β1-β2 and β6-β7 loops (31). The Itk PHD interacts with CaM via β3-β4 and β5-β6 loops (84). Altogether, in Akt, Itk, and Grb7, the mode of PHDs binding to CaM deviates from that involving helical structures. Here, our modeling and simulation results indicate the CaM-PHD association being thermodynamically stable and being maintained by strong intermolecular H-bonds, salt bridges, and polar and nonpolar interactions. CaM contains nine critical Met residues located in the N-lobe, the central α-helix, and the C-lobe. Met residues M109, M124, M144, and M145 in the CaM C-lobe form a hydrophobic region essential for hydrophobic interaction with the hydrophobic residues I19, W22, and W80 in the PHD. Based on the MD trajectories analyses, we propose four models for dimeric representations of CaM-PHD association. We observe that the C-lobe of CaM is critical for the binding. The central helix region and the weakly binding N-lobe of CaM also play a role in binding, especially in the absence of IP_4. When IP_4 is loaded onto the PHD, the interactions between CaM-PHD become weaker; the N-lobe of CaM easily dissociates when IP_4 interferes with the interaction at the C-lobe of CaM, hence weakening the overall interactions. We cluster the trajectories and present the most populated state for each proposed model and the key interactions that are essential for maintaining the dimeric complexes.

CONCLUSION

Akt activation mechanisms have been proposed. Here, we provide detailed conformational views into how CaM binds to the Akt PHD at the atomic level and the involvement of IP_4 in the CaM-PHD complex, which weakens or partially displaces CaM. Akt is recruited to the plasma membrane by specific interactions between its PHD and CaM and PIP_3, a phospholipid found in the plasma membrane that serves as the docking site of Akt (18,24). The binding mode of CaM to the Akt PHD was established by NMR experiments, and the observations by both the NMR and our simulations deviate from CaM's typical binding mode, which usually involves α-helices (67,68). Our results suggest that CaM binds to the β-sheets in the Akt PHD, which is rare, but such binding has been reported by another NMR study as well, in which CaM bound to the Itk PHD (84). Mechanistically, CaM's N- and C-terminal lobes and the central linker simultaneously engage the Akt PHD. The Akt PHD binds to one end of CaM, especially the C-lobe, and induces conformational rearrangements engaging the central linker and the N-lobe. Further, our docking and simulation results enable us to select and propose four models (Configs. 1, 2, 3, and 5) of CaM-PHD dimeric complexes, showing the β-sheets in the Akt PHD binding to CaM. A high percentage of the NMR chemical shift residues were observed in the interface, and most of these residues play an important role in maintaining the dimeric CaM-PHD complex. The most populated state of each proposed model, as well as key intermolecular interactions that are cardinal to maintain the dimeric complex CaM-PHD, is presented. Also, the PC1 vs. PC2 conformer plots, scree plots, and collective motions defined by PC1 for all eight models succinctly revealed essential conformational changes or essential dynamics that were sampled throughout the MD simulations.

Our models reveal how IP_4 acts by weakening or partially displacing CaM, thereby revealing the detailed molecular basis of Akt translocation, phosphorylation, and activation. They may also serve as a guide for future research on CaM-PHD association or serve as a basis for drug development to disrupt the CaM-PHD complex.

SUPPORTING MATERIAL

Supporting material can be found online at https://doi.org/10.1016/j.bpj.2021.03.018.

AUTHOR CONTRIBUTIONS

J.W. performed MD simulations, investigated, analyzed data, and wrote the manuscript. H.J., O.K., A.G., and R.N. conceptualized the methodology, analyzed, investigated, validated, reviewed, and edited manuscript.

ACKNOWLEDGMENTS

J.W. acknowledges the Scientific and Technological Research Council of Turkey for partially supporting this project through the 2235- Graduate Scholarship for Least Developed Countries. This project has been funded in whole or in part with federal funds from the National Cancer Institute, National Institutes of Health (NIH), under contract HHSN261200800001E. The content of this publication does not necessarily reflect the views or policies of the Department of Health and Human Services, nor does mention of trade names, commercial products or organizations imply endorsement by the US Government. This research was supported in part by the Intramural Research Program of the NIH, National Cancer Institute, Center for Cancer Research, and the Intramural Research Program of the NIH Clinical Center. All simulations were performed using the high-performance computational facilities of the Biowulf PC/Linux cluster at the NIH, Bethesda, MD (https://hpc.nih.gov/).

REFERENCES

1. Leroux, A. E., J. O. Schulze, and R. M. Biondi. 2018. AGC kinases, mechanisms of regulation and innovative drug development. *Semin. Cancer Biol.* 48:1–17.
2. Pearce, L. R., D. Komander, and D. R. Alessi. 2010. The nuts and bolts of AGC protein kinases. *Nat. Rev. Mol. Cell Biol.* 11:9–22.
3. Altomare, D. A., and J. R. Testa. 2005. Perturbations of the AKT signaling pathway in human cancer. *Oncogene.* 24:7455–7464.
4. Coticchia, C. M., C. M. Revankar, …, M. D. Johnson. 2009. Calmodulin modulates Akt activity in human breast cancer cell lines. *Breast Cancer Res. Treat.* 115:545–560.
5. Pérez-Tenorio, G., O. Stål; Southeast Sweden Breast Cancer Group. 2002. Activation of AKT/PKB in breast cancer predicts a worse outcome among endocrine treated patients. *Br. J. Cancer.* 86: 540–545.
6. Cristiano, B. E., J. C. Chan, …, R. B. Pearson. 2006. A specific role for AKT3 in the genesis of ovarian cancer through modulation of G(2)-M phase transition. *Cancer Res.* 66:11718–11725.
7. Héron-Milhavet, L., C. Franckhauser, …, N. J. Lamb. 2006. Only Akt1 is required for proliferation, while Akt2 promotes cell cycle exit through p21 binding. *Mol. Cell. Biol.* 26:8267–8280.
8. Irie, H. Y., R. V. Pearline, …, J. S. Brugge. 2005. Distinct roles of Akt1 and Akt2 in regulating cell migration and epithelial-mesenchymal transition. *J. Cell Biol.* 171:1023–1034.
9. Yun, S. J., D. F. Tucker, …, S. S. Bae. 2009. Differential regulation of Akt/protein kinase B isoforms during cell cycle progression. *FEBS Lett.* 583:685–690.
10. Carpten, J. D., A. L. Faber, …, J. E. Thomas. 2007. A transforming mutation in the pleckstrin homology domain of AKT1 in cancer. *Nature.* 448:439–444.
11. Lindhurst, M. J., J. C. Sapp, …, L. G. Biesecker. 2011. A mosaic activating mutation in AKT1 associated with the Proteus syndrome. *N. Engl. J. Med.* 365:611–619.
12. Cho, H., J. Mu, …, M. J. Birnbaum. 2001. Insulin resistance and a diabetes mellitus-like syndrome in mice lacking the protein kinase Akt2 (PKB beta). *Science.* 292:1728–1731.
13. George, S., J. J. Rochford, …, I. Barroso. 2004. A family with severe insulin resistance and diabetes due to a mutation in AKT2. *Science.* 304:1325–1328.
14. Easton, R. M., H. Cho, …, M. J. Birnbaum. 2005. Role for Akt3/protein kinase Bgamma in attainment of normal brain size. *Mol. Cell. Biol.* 25:1869–1878.
15. Hanada, M., J. Feng, and B. A. Hemmings. 2004. Structure, regulation and function of PKB/AKT–a major therapeutic target. *Biochim. Biophys. Acta.* 1697:3–16.
16. Liao, Y., and M. C. Hung. 2010. Physiological regulation of Akt activity and stability. *Am. J. Transl. Res.* 2:19–42.
17. Fruman, D. A., H. Chiu, …, R. T. Abraham. 2017. The PI3K pathway in human disease. *Cell.* 170:605–635.
18. Dillon, R. L., D. E. White, and W. J. Muller. 2007. The phosphatidyl inositol 3-kinase signaling network: implications for human breast cancer. *Oncogene.* 26:1338–1345.
19. Franke, T. F. 2008. Intracellular signaling by Akt: bound to be specific. *Sci. Signal.* 1:pe29.
20. Franke, T. F., S. I. Yang, …, P. N. Tsichlis. 1995. The protein kinase encoded by the Akt proto-oncogene is a target of the PDGF-activated phosphatidylinositol 3-kinase. *Cell.* 81:727–736.
21. Miao, B., and A. Degterev. 2011. Targeting phospshatidylinositol 3-kinase signaling with novel phosphatidylinositol 3,4,5-triphosphate antagonists. *Autophagy.* 7:650–651.
22. Yap, T. A., M. D. Garrett, …, P. Workman. 2008. Targeting the PI3K-AKT-mTOR pathway: progress, pitfalls, and promises. *Curr. Opin. Pharmacol.* 8:393–412.
23. Agamasu, C., R. H. Ghanam, …, J. S. Saad. 2017. The interplay between calmodulin and membrane interactions with the pleckstrin homology domain of Akt. *J. Biol. Chem.* 292:251–263.
24. Cooray, S. 2004. The pivotal role of phosphatidylinositol 3-kinase-Akt signal transduction in virus survival. *J. Gen. Virol.* 85:1065–1076.
25. Manning, B. D., and A. Toker. 2017. AKT/PKB signaling: navigating the network. *Cell.* 169:381–405.
26. Milburn, C. C., M. Deak, …, D. M. Van Aalten. 2003. Binding of phosphatidylinositol 3,4,5-trisphosphate to the pleckstrin homology domain of protein kinase B induces a conformational change. *Biochem. J.* 375:531–538.
27. Lučić, I., M. K. Rathinaswamy, …, T. A. Leonard. 2018. Conformational sampling of membranes by Akt controls its activation and inactivation. *Proc. Natl. Acad. Sci. USA.* 115:E3940–E3949.
28. James, S. R., C. P. Downes, …, D. R. Alessi. 1996. Specific binding of the Akt-1 protein kinase to phosphatidylinositol 3,4,5-trisphosphate without subsequent activation. *Biochem. J.* 315:709–713.
29. Chu, N., A. L. Salguero, …, P. A. Cole. 2018. Akt kinase activation mechanisms revealed using protein semisynthesis. *Cell.* 174:897–907.e14.
30. Sarbassov, D. D., D. A. Guertin, …, D. M. Sabatini. 2005. Phosphorylation and regulation of Akt/PKB by the rictor-mTOR complex. *Science.* 307:1098–1101.
31. Agamasu, C., R. H. Ghanam, and J. S. Saad. 2015. Structural and biophysical characterization of the interactions between calmodulin and the pleckstrin homology domain of Akt. *J. Biol. Chem.* 290:27403–27413.
32. Huang, B. X., M. Akbar, …, H. Y. Kim. 2011. Phosphatidylserine is a critical modulator for Akt activation. *J. Cell Biol.* 192:979–992.
33. Calleja, V., M. Laguerre, …, B. Larijani. 2009. Role of a novel PH-kinase domain interface in PKB/Akt regulation: structural mechanism for allosteric inhibition. *PLoS Biol.* 7:e17.
34. Wu, W. I., W. C. Voegtli, …, B. J. Brandhuber. 2010. Crystal structure of human AKT1 with an allosteric inhibitor reveals a new mode of kinase inhibition. *PLoS One.* 5:e12913.
35. Calleja, V., D. Alcor, …, B. Larijani. 2007. Intramolecular and intermolecular interactions of protein kinase B define its activation in vivo. *PLoS Biol.* 5:e95.

36. Parikh, C., V. Janakiraman, …, S. Seshagiri. 2012. Disruption of PH-kinase domain interactions leads to oncogenic activation of AKT in human cancers. *Proc. Natl. Acad. Sci. USA.* 109:19368–19373.

37. Deb, T. B., C. M. Coticchia, and R. B. Dickson. 2004. Calmodulin-mediated activation of Akt regulates survival of c-Myc-overexpressing mouse mammary carcinoma cells. *J. Biol. Chem.* 279:38903–38911.

38. Zhang, M., H. Jang, and R. Nussinov. 2019. The mechanism of PI3Kα activation at the atomic level. *Chem. Sci. (Camb.).* 10:3671–3680.

39. Zhang, M., H. Jang, and R. Nussinov. 2019. The structural basis for Ras activation of PI3Kα lipid kinase. *Phys. Chem. Chem. Phys.* 21:12021–12028.

40. Hsieh, T. C., C. Y. Lin, …, J. M. Wu. 2014. Biochemical and cellular evidence demonstrating AKT-1 as a binding partner for resveratrol targeting protein NQO2. *PLoS One.* 9:e101070.

41. Luo, Y., A. R. Shoemaker, …, V. L. Giranda. 2005. Potent and selective inhibitors of Akt kinases slow the progress of tumors in vivo. *Mol. Cancer Ther.* 4:977–986.

42. Berman, H. M., T. Battistuz, …, C. Zardecki. 2002. The Protein Data Bank. *Acta Crystallogr. D Biol. Crystallogr.* 58:899–907.

43. Schenkelberg, C. D., and C. Bystroff. 2015. InteractiveROSETTA: a graphical user interface for the PyRosetta protein modeling suite. *Bioinformatics.* 31:4023–4025.

44. BIOVIA Dassault Systeme. 2016. Discovery studio modelling environment, release 2017. Dassault Systeme, San Diego, CA.

45. Hubbard, S. J., and J. M. Thornton. 1993. NACCESS computer program version 2.1.1. Department of Biochemistry and Molecular Biology, University College, London, UK.

46. Baspinar, A., E. Cukuroglu, …, A. Gursoy. 2014. PRISM: a web server and repository for prediction of protein-protein interactions and modeling their 3D complexes. *Nucleic Acids Res.* 42:W285–W289.

47. DeLano, W. L. 2002. The PyMOL molecular graphics system. DeLano Scientific, San Carlos, CA.

48. Brooks, B. R., C. L. Brooks, III, …, M. Karplus. 2009. CHARMM: the biomolecular simulation program. *J. Comput. Chem.* 30:1545–1614.

49. Klauda, J. B., R. M. Venable, …, R. W. Pastor. 2010. Update of the CHARMM all-atom additive force field for lipids: validation on six lipid types. *J. Phys. Chem. B.* 114:7830–7843.

50. Chakrabarti, M., H. Jang, and R. Nussinov. 2016. Comparison of the conformations of KRAS isoforms, K-Ras4A and K-Ras4B, points to similarities and significant differences. *J. Phys. Chem. B.* 120:667–679.

51. Jang, H., S. Muratcioglu, …, R. Nussinov. 2016. Membrane-associated Ras dimers are isoform-specific: K-Ras dimers differ from H-Ras dimers. *Biochem. J.* 473:1719–1732.

52. Muratcioglu, S., H. Jang, …, R. Nussinov. 2017. PDEδ binding to Ras isoforms provides a route to proper membrane localization. *J. Phys. Chem. B.* 121:5917–5927.

53. Jang, H., A. Banerjee, …, R. Nussinov. 2017. Flexible-body motions of calmodulin and the farnesylated hypervariable region yield a high-affinity interaction enabling K-Ras4B membrane extraction. *J. Biol. Chem.* 292:12544–12559.

54. Zhang, M., H. Jang, …, R. Nussinov. 2017. Phosphorylated calmodulin promotes PI3K activation by binding to the SH_2 domains. *Biophys. J.* 113:1956–1967.

55. Ozdemir, E. S., H. Jang, …, R. Nussinov. 2018. Unraveling the molecular mechanism of interactions of the Rho GTPases Cdc42 and Rac1 with the scaffolding protein IQGAP2. *J. Biol. Chem.* 293:3685–3699.

56. Ozdemir, E. S., H. Jang, …, R. Nussinov. 2018. Arl2-Mediated allosteric release of farnesylated KRas4B from shuttling factor PDEδ. *J. Phys. Chem. B.* 122:7503–7513.

57. Liao, T. J., H. Jang, …, R. Nussinov. 2018. Allosteric KRas4B can modulate SOS1 fast and slow Ras activation cycles. *Biophys. J.* 115:629–641.

58. Zhang, M., Z. Li, …, R. Nussinov. 2018. Calmodulin (CaM) activates PI3Kα by targeting the "soft" CaM-binding motifs in both the nSH2 and cSH2 domains of p85α. *J. Phys. Chem. B.* 122:11137–11146.

59. Jang, H., A. Banerjee, …, R. Nussinov. 2019. The structural basis of the farnesylated and methylated KRas4B interaction with calmodulin. *Structure.* 27:1647–1659.e1644.

60. Zhang, M., Z. Li, …, R. Nussinov. 2019. Ca^{2+}-Dependent switch of calmodulin interaction mode with tandem IQ motifs in the scaffolding protein IQGAP1. *Biochemistry.* 58:4903–4911.

61. Phillips, J. C., R. Braun, …, K. Schulten. 2005. Scalable molecular dynamics with NAMD. *J. Comput. Chem.* 26:1781–1802.

62. Im, W., M. S. Lee, and C. L. Brooks, III. 2003. Generalized born model with a simple smoothing function. *J. Comput. Chem.* 24:1691–1702.

63. Pettersen, E. F., T. D. Goddard, …, T. E. Ferrin. 2004. UCSF Chimera–a visualization system for exploratory research and analysis. *J. Comput. Chem.* 25:1605–1612.

64. Grant, B. J., A. P. Rodrigues, …, L. S. Caves. 2006. Bio3d: an R package for the comparative analysis of protein structures. *Bioinformatics.* 22:2695–2696.

65. Han, B., Y. Liu, …, D. S. Wishart. 2011. SHIFTX2: significantly improved protein chemical shift prediction. *J. Biomol. NMR.* 50:43–57.

66. Tuncbag, N., O. Keskin, and A. Gursoy. 2010. HotPoint: hot spot prediction server for protein interfaces. *Nucleic Acids Res.* 38:W402–W406.

67. Vetter, S. W., and E. Leclerc. 2003. Novel aspects of calmodulin target recognition and activation. *Eur. J. Biochem.* 270:404–414.

68. Villarroel, A., M. Taglialatela, …, P. Areso. 2014. The ever changing moods of calmodulin: how structural plasticity entails transductional adaptability. *J. Mol. Biol.* 426:2717–2735.

69. Abdi, H., and L. J. Williams. 2010. Principal component analysis. *Wiley Interdiscip. Rev. Comput. Stat.* 2:433–459.

70. Balsera, M. A., W. Wriggers, …, K. Schulten. 1996. Principal component analysis and long time protein dynamics. *J. Phys. Chem.* 100:2567–2572.

71. David, C. C., and D. J. Jacobs. 2014. Principal component analysis: a method for determining the essential dynamics of proteins. *Methods Mol. Biol.* 1084:193–226.

72. Grant, B. J., L. Skjaerven, and X. Q. Yao. 2021. The Bio3D packages for structural bioinformatics. *Protein Sci.* 30:20–30.

73. Lemmon, M. A. 2007. Pleckstrin homology (PH) domains and phosphoinositides. *Biochem. Soc. Symp.* 74:81–93.

74. Xu, Q., A. Bateman, …, I. A. Wilson. 2010. Bacterial pleckstrin homology domains: a prokaryotic origin for the PH domain. *J. Mol. Biol.* 396:31–46.

75. Yu, J. W., J. M. Mendrola, …, M. A. Lemmon. 2004. Genome-wide analysis of membrane targeting by *S. cerevisiae* pleckstrin homology domains. *Mol. Cell.* 13:677–688.

76. Chin, D., and A. R. Means. 2000. Calmodulin: a prototypical calcium sensor. *Trends Cell Biol.* 10:322–328.

77. Tidow, H., and P. Nissen. 2013. Structural diversity of calmodulin binding to its target sites. *FEBS J.* 280:5551–5565.

78. Garrido, E., J. Lázaro, …, J. Rubio-Martinez. 2018. Modeling and subtleties of K-Ras and Calmodulin interaction. *PLOS Comput. Biol.* 14:e1006552.

79. Ni, D., D. Liu, …, S. Lu. 2018. Computational insights into the interactions between calmodulin and the c/nSH2 domains of p85α regulatory subunit of PI3Kα: implication for PI3Kα activation by calmodulin. *Int. J. Mol. Sci.* 19:151.

80. Aykut, A. O., A. R. Atilgan, and C. Atilgan. 2013. Designing molecular dynamics simulations to shift populations of the conformational states of calmodulin. *PLOS Comput. Biol.* 9:e1003366.

81. Kurkcuoglu, Z., I. Bahar, and P. Doruker. 2016. ClustENM: ENM-based sampling of essential conformational space at full atomic resolution. *J. Chem. Theory Comput.* 12:4549–4562.

82. Dong, B., C. A. Valencia, and R. Liu. 2007. Ca(2+)/calmodulin directly interacts with the pleckstrin homology domain of AKT1. *J. Biol. Chem.* 282:25131–25140.

83. Ishida, H., and H. J. Vogel. 2006. Protein-peptide interaction studies demonstrate the versatility of calmodulin target protein binding. *Protein Pept. Lett.* 13:455–465.

84. Wang, X., S. E. Boyken, …, Y. H. Huang. 2014. Calmodulin and PI(3,4,5)P_3 cooperatively bind to the Itk pleckstrin homology domain to promote efficient calcium signaling and IL-17A production. *Sci. Signal.* 7:ra74.

85. Watson, G. M., and J. A. Wilce. 2020. Direct interaction between calmodulin and the Grb7 RA-PH domain. *Int. J. Mol. Sci.* 21:1336.